IOP Conf. Series: Journal of Physics: Conf. Series **874** (2017) 012040 doi:10.1088/1742-6596/874/1/012040

Simulation of DLA grating structures in the frequency domain

T Egenolf[1], O Boine-Frankenheim[1,2] and U Niedermayer[1]

[1] TEMF, TU Darmstadt, Schlossgartenstr. 8, 64289 Darmstadt
[2] GSI, Planckstr. 1, 64291 Darmstadt

E-mail: egenolf@temf.tu-darmstadt.de

Abstract. Dielectric laser accelerators (DLA) driven by ultrashort laser pulses can reach orders of magnitude larger gradients than contemporary RF electron accelerators. A new implemented field solver based on the finite element method in the frequency domain allows the efficient calculation of the structure constant, i.e. the ratio of energy gain to laser peak amplitude. We present the maximization of this ratio as a parameter study looking at a single grating period only. Based on this optimized shape the entire design of a beta-matched grating is completed in an iterative process. The period length of a beta-matched grating increases due to the increasing velocity of the electron when a subrelativistic beam is accelerated. The determination of the optimal length of each grating period thus requires the knowledge of the energy gain within all so far crossed periods. Furthermore, we outline to reverse the excitation in the presented solver for beam coupling impedance calculations and an estimation of the beam loading intensity limit.

1. Introduction

Several applications of particle accelerators request higher acceleration gradients than delivered by current rf-accelerators for more compact devices. Dielectric laser accelerators (DLAs) [1] are potential candidates for advanced linear electron accelerators with gradients in the range of GeV/m. In the future, such compact DLAs will provide the opportunity for compact radiotherapy devices and free electron lasers, for example.

Recently, DLA experiments have demonstrated acceleration gradients of about 376 MeV/m for subrelativistic electrons and acceleration gradients of about 690 MeV/m for relativistic beams at SLAC [2].

In these experiments, electrical near-fields of pulsed solid state lasers modulated by dielectric nanostructures are used to accelerate electrons. The structures are fabricated by lithographic techniques. Of particular interest for characterizing such periodic structures is the maximum reachable acceleration gradient expressed by the structure constant

$$SC = \frac{\max\left(\Delta W\right)}{eE_0\lambda_{gz}} = |\underline{e}_\mathrm{n}| \tag{1}$$

with the energy gain ΔW of an electron passing through period of length λ_{gz} in positive z-direction. The driving (z-polarized) laser with peak amplitude E_0 propagates in y-direction and

the longitudinal electric laser field $\underline{E}_z$ in the frequency domain is expanded in a spatial Fourier series with the normalized harmonic coefficients

$$\underline{e}_{\mathrm{n}} = \frac{1}{E_0 \lambda_{gz}} \int_{-\lambda_{gz}/2}^{\lambda_{gz}/2} \underline{E}_{\mathrm{z}} e^{\mathrm{in}\frac{2\pi}{\lambda_{gz}}z} dz. \tag{2}$$

In order to calculate the Fourier coefficients, we implemented a simulation tool based on the finite element method in 2D on an unstructured triangular mesh using FEniCS [3], an open-source toolbox for automated solution of PDEs. The mesh originates from Gmsh [4] and is imported via DOLFIN-CONVERT [5]. The advantage of such a mesh is a better adaptability to curved geometries than a hexahedral mesh commonly used in time domain simulations. Since most of the DLA structures are translation invariant in one direction, two-dimensional simulations suffice at the first design stage.

2. 2D FEM field solver

The fields $\underline{\mathbf{E}} : \Omega \subset \mathbb{R}^2 \to \mathbb{C}^2$ required to calculate the Fourier coefficients are solutions of the curl-curl-equation

$$\nabla \times \left[\mu_0^{-1} \nabla \times \underline{\mathbf{E}}\right] - \omega^2 \varepsilon \underline{\mathbf{E}} = -\mathrm{i}\omega \underline{\mathbf{J}} \tag{3}$$

with the permeability constant μ_0 and the permittivity $\varepsilon = \varepsilon_0 \varepsilon_{\mathrm{r}}(y, z)$ as a function of position. The current density $\underline{\mathbf{J}}$ models the incident laser and is imprinted as a constant on a small stripe of the mesh outside the dielectric.

Testing with functions $\underline{\mathbf{v}}_i \in \mathrm{H}_{\mathrm{2D}}^{\mathrm{curl}}$, where $\mathrm{H}_{\mathrm{2D}}^{\mathrm{curl}}$ is the Sobolev space of square integrable functions with square integrable two dimensional curl, results in the weak formulation

$$\int_\Omega \left[\mu_0^{-1} \left\{\nabla \times \underline{\mathbf{E}}\right\} \cdot \left\{\nabla \times \underline{\mathbf{v}}\right\} - \omega^2 \varepsilon \underline{\mathbf{E}} \cdot \underline{\mathbf{v}}\right] d\Omega - \int_{\partial\Omega} \left[\mu_0^{-1} \left\{\nabla \times \underline{\mathbf{E}}\right\} \times \mathbf{n}\right] \cdot \underline{\mathbf{v}} ds = -\int_\Omega \mathrm{i}\omega \underline{\mathbf{J}} \cdot \underline{\mathbf{v}} d\Omega \tag{4}$$

with the outward unit vector $\mathbf{n}$ normal to the boundary $\partial\Omega$. The Galerkin ansatz

$$\underline{\mathbf{E}} = \sum_n a_n \underline{\mathbf{v}}_n \tag{5}$$

with degrees of freedom a_n and Nédélec edge elements $\underline{\mathbf{v}}_n$ [6] provides a linear equation system which is solved numerically.

A periodic boundary condition is applied on the boundary normal to the beam path. Two different boundary conditions can be chosen on the lateral sides: a Sommerfeld boundary condition [7]

$$\mathbf{n} \times (\nabla \times \underline{\mathbf{E}}) = -\mathrm{i}\omega c^{-1} \mathbf{n} \times (\mathbf{n} \times \underline{\mathbf{E}}) \tag{6}$$

or a perfectly matched layer [8].

3. Simulation examples

The new simulation tool has various applications in the design of DLA structures. We analyze a new "slightly resonant" silicon structure ($\varepsilon_{\mathrm{r}} = 11.63$) which is proposed in [9]. The design is called cavity structure in the following. The structure constant depends significantly on the values of three geometry parameters depicted in the schematic drawing in Figure 1.

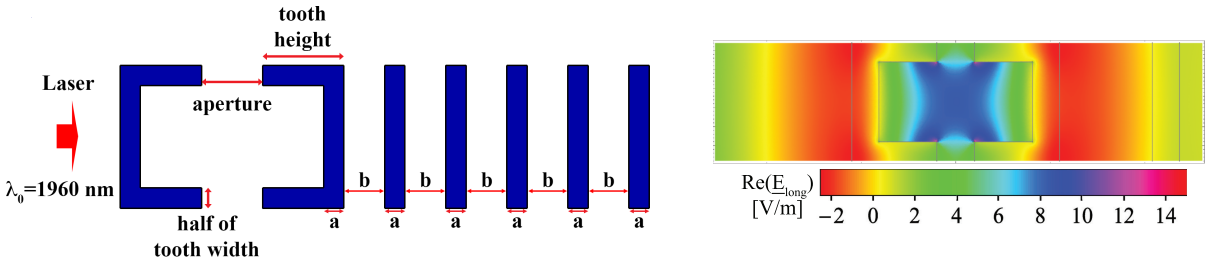

Figure 1. Schematic drawing and longitudinal electric field of the cavity structure. The thickness of the layers is given by the Bragg condition $a = \lambda_0/\left(4\sqrt{\varepsilon_r}\right)$ and $b = \lambda_0/4$ with $\varepsilon_r = 11.63$ and the beam path is in the middle of the aperture. The laser strength of the plotted field is 1 V/m.

3.1. Single period optimization

Parameter studies can be used to optimize the structure constant of a single period. Since the structure constant increases as the aperture decreases, an aperture of 200 nm is a trade-off between maximum reachable structure constant and maximum admissible transversal beam size. The absolute value of the structure constant depending on the remaining parameters, width and height of the tooth, is shown in Figure 2. Choosing a width of 200 nm and a height of 450 nm results in a maximum structure constant of about 0.74 for a period length of 620 nm (cross-checked by CST® time domain simulations, see [9]). In the choice of electron beam parameters we follow [10], i.e. $\beta = 0.3165$.

Furthermore, longer periods, corresponding to larger velocities, can reach much larger structure constants. The maximum structure constant for a period length of 1800 nm is about 2.1, for example. The geometry parameters of such a period are an aperture of 400 nm and a tooth width of 550 nm and height of 450 nm (see Figure 3).

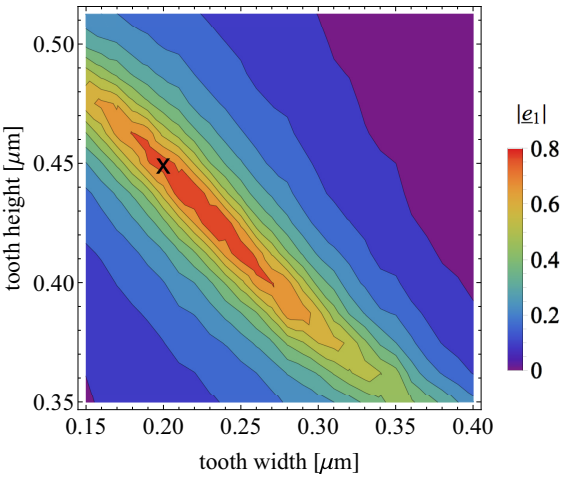

Figure 2. Parameter study of the structure constant for a period length of 620 nm. The X symbolizes the geometry parameters with the maximum structure constant.

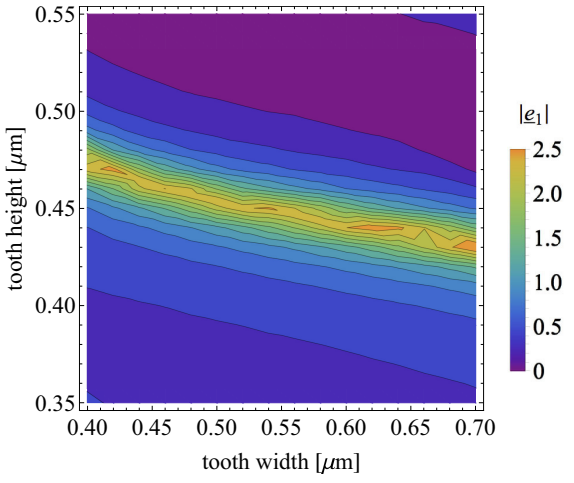

Figure 3. Parameter study of the structure constant for a period length of 1800 nm.

First prototypes of the proposed cavity structure are now being fabricated. Since 90° corners are not feasible by lithographic etching techniques, the corners in the original design have to be rounded with a minimum radius of 50 nm. Such restrictions can be integrated in simulations by modifying the mesh (see Figure 4). The structure constant is thus reduced to about 0.63 at the geometry parameters optimized before for a 620 nm period. A new maximum of 0.66 can be reached at a tooth width of 240 nm and height of 425 nm.

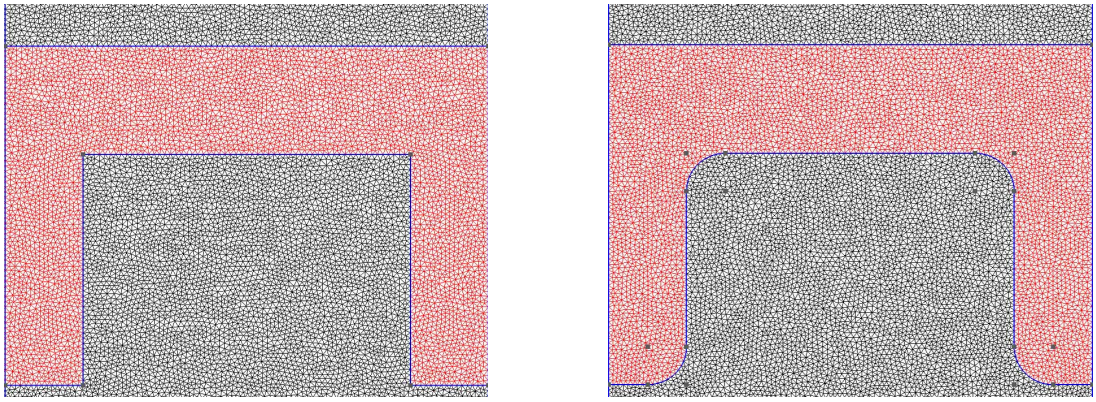

Figure 4. Comparison of the triangular mesh with 90° corners on the left and rounded corners on the right. The upper half of the cavity structure is shown.

3.2. Designing a beta-matched grating

Due to the phase synchronicity condition $\lambda_{gz} = n\beta\lambda_0$, where n is the spatial harmonic, the period length along a grating has to increase for an increasing particle velocity. The energy gain per period of the synchronous particle is

$$\Delta W = eE_0\lambda_{gz}|\underline{e}_\mathrm{n}|\cos(\varphi_s)\,, \tag{7}$$

where $\varphi_s = \varphi_\mathrm{p} + \arg(\underline{e}_\mathrm{n})$ and the phase φ_p of the particle is referred to the laser phase. Since φ_p is constant along the beta-matched grating, the phase of the n-th Fourier coefficient also needs to be as constant as possible in order to accelerate in stable buckets.

3.2.1. Phase stabilization. An increase in period length along a beta-matched grating only is not sufficient since this changes the phase of the Fourier coefficient significantly. As shown in Figure 5, the change in $\arg(\underline{e}_1)$ is in the range of 30°, which may lead to particle loss. If the width of the teeth is adjusted as well, the phase drift can be limited to about 4°. Here, the tooth width is optimized as linear function of the period length

$$t(\lambda_{gz}) = t^{(0)}\left(\frac{\lambda_{gz}/\lambda_{gz}^{(0)} - 1}{\xi} + 1\right), \tag{8}$$

where $t^{(0)} = 200\,\mathrm{nm}$, $\lambda_{gz}^{(0)} = 620\,\mathrm{nm}$ and $\xi \approx 2.7$. Moreover, the decrease of the structure constant is also reduced from 33 % to 17 %.

3.2.2. Iterative approach. Finally, an iterative approach can be used to construct such a beta-matched grating. The optimized design of one period forms the basis of the approach. Since the velocity of a reference electron in a grating period depends on the energy gain in all previous periods, an iterative design process is to be favored. As an example we present a beta-matched grating based on the proposed cavity structure and further informations on the approach in [9].

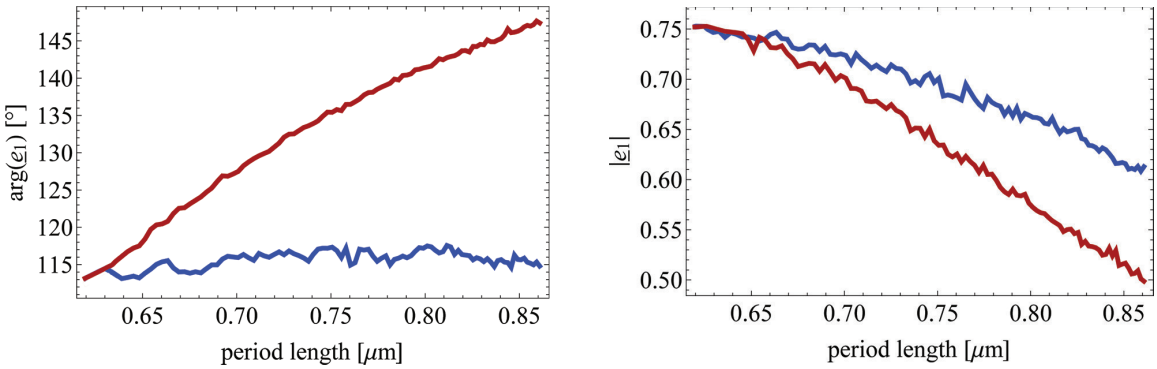

Figure 5. Phase and absolute value of the First Fourier coefficient over the period length for constant tooth width (red) and adapted tooth width according to Equation (8) (blue).

4. Conclusion

The solver described in this contribution calculates the electric field in DLA nanostructures based on the finite element method in the frequency domain and predicts the structure constant. The solver can be integrated in the design process of 2D structures, performing all necessary simulations for a beta-matched grating.

Simulations in the frequency domain require the solution of one linear matrix equation per calculation of a structure constant in contrast to simulations in the time domain, which require one matrix multiplication per time step. Furthermore, the use of a triangular mesh is favorable in the frequency domain. This makes the solver advantageous for simulations of curved geometries.

A further application of the solver is the estimation of the beam loading limit for DLA structures. Therefore, the excitation is shifted to the beam path to calculate the beam coupling impedance. The wake potential can then be obtained by a discrete Fourier transform of the impedance and a convolution with the beam distribution. This upgrade is presently under development.

Acknowledgments

This work is supported by the Gordon and Betty Moore Foundation under grant GBMF4744 and the German Federal Ministry of Education and Research under grant FKZ:05K16RDB.

References

[1] Peralta E A et al 2013 Demonstration of electron acceleration in a laser-driven dielectric microstructure *Nature* **503** 91–94
[2] Wootton K P, McNeur J and Leedle K J 2016 Dielectric laser accelerators: designs, experiments, and applications *Rev. Accl. Sci. Tech.* **9** 105–26
[3] Logg A, Mardal K-A and Wells G N 2012 *Automated Solution of Differential Equations by the Finite Element Method* (Berlin: Springer)
[4] Geuzaine C and Remacle J-F 2009 Gmsh: a 3-D finite element mesh generator with built-in pre- and post-processing facilities *Int. J. Numer. Meth. Engng.* **79** 1309–31
[5] Logg A and Wells G N 2010 DOLFIN: automated finite element computing *ACM Transactions on Mathematical Software* **37** 20
[6] Nédélec J C 1980 Mixed finite elements in $\mathbb{R}^3$ *Numerische Mathematik* **35** 315–41
[7] Jin J-M and Riley D J 2009 *Finite Element Analysis of Antennas and Arrays* (Hoboken: Wiley)
[8] Sacks Z S, Kingsland D M, Lee R and Lee J F 1995 A perfectly matched anisotropic absorber for use as an absorbing boundary condition *IEEE Trans. Antennas Propagat.* **43** 1460–64
[9] Niedermayer U, Boine-Frankenheim O and Egenolf T 2017 Designing a dielectric laser accelerator on a chip *Proc. 8th Int. Particle Accelerator Conf. (May 14–19 Copenhagen)* WEPVA003
[10] Breuer J and Hommelhoff P 2013 Laser-based acceleration of nonrelativistic electrons at a dielectric structure *Phys. Rev. Lett.* **111** 134803